

1

An examination of the high-order dynamic interactions 2 underlying multi-dimensional timeseries data

3 Lucy L. W. Owen¹, Thomas Hao Chang^{1,2}, and Jeremy R. Manning^{1,†}

¹Department of Psychological and Brain Sciences,
Dartmouth College, Hanover, NH

³Amazon.com, Seattle, WA

[†]Address correspondence to jeremy.r.manning@dartmouth.edu

4 March 26, 2019

5 **Abstract**

6 Most complex systems reflect dynamic interactions between myriad evolving components (e.g., interacting
7 molecules, interacting brain systems, interacting individuals within a social network or ecological
8 system, coordinated components within a mechanical or digital device, etc.). Despite that these interactions
9 are central to the full system’s behavior (e.g., removing a component from the full system can change the
10 entire system’s behavior), dynamic interactions cannot typically be directly measured. Rather, the interactions
11 must be inferred through their hypothesized role in guiding the dynamics of system components.
12 Here we use a model-based approach to inferring dynamic interactions from timeseries data. In addition
13 to examining first-order interactions (e.g., between pairs of components) we also examine higher-order
14 interactions (e.g., that characterize mirrored structure in the patterns of interaction dynamics displayed
15 by different subsets of components). We apply our approach to two datasets. First, we use a synthetic
16 dataset, for which the underlying dynamic interactions are known, to show that our model recovers those
17 ground-truth dynamic interactions. We also apply our model to a neuroimaging dataset and show that the
18 high-order dynamic interactions exhibited by brain data vary meaningfully as a function of the cognitive
19 “richness” of the stimulus people are experiencing.

20 **Introduction**

21 The dynamics of the observable universe are meaningful in three respects. First, the behaviors of the *atomic*
22 *units* that exhibit those dynamics are highly interrelated. The actions of one unit typically have implications
23 for one or more other units. In other words, there is non-trivial *correlational structure* defining how different
24 units interact with and relate to each other. Second, that correlational structure is *hierarchical* in the sense
25 that it exists on many spatiotemporal scales. The way one group of units interacts may relate to how another
26 group of units interact, and the interactions between those groups may exhibit some rich structure. Third,
27 the structure at each level of this correlational hierarchy changes from moment to moment, reflecting the
28 “behavior” of the full system.

29 These three properties (rich correlations, hierarchical organization, and dynamics) are major hallmarks
30 of many complex systems. For example, within a single cell, the cellular components interact at many

31 spatiotemporal scales, and those interactions change according to what that single cell is doing. Within a
32 single human brain, the individual neurons interact within each brain structure, and the structures interact
33 to form complex networks. The interactions at each scale vary according to the functions our brains are
34 carrying out. And within social groups, interactions at different scales (e.g., between individuals, family
35 units, communities, etc.) vary over time according to changing goals and external constraints.

36 Although many systems exhibit rich dynamic correlations at many scales, a major challenge to studying
37 such patterns is that typically neither the correlations nor the hierarchical organizations of those correlations
38 may be directly observed. Rather, these fundamental properties must be inferred indirectly by examining
39 the observable parts of the system— e.g., the behaviors of the individual atomic units of that system. In
40 the *Methods* section, we propose a series of mathematical operations that may be used to recover dynamic
41 correlations at a range of scales (i.e., orders of interaction). In the *Results* section, we demonstrate how our
42 approach may be applied to multi-dimensional timeseries data: a synthetic dataset where the underlying
43 dynamic correlations are known (we use this dataset to validate our approach), and a neuroimaging dataset
44 comprising data collected as participants listened to a story (Simony et al., 2016). In different experimental
45 conditions in the neuroimaging study, participants listened to altered versions of the story that varied in
46 cognitive richness: the intact story (fully engaging), a scrambled version of the story where the paragraphs
47 were presented in a randomized order (moderately engaging), a second scrambled condition where the
48 words were presented in a random order (minimally engaging), and a “rest” condition where the participants
49 did not listen to any version of the story (control condition). We use the neuroimaging dataset to examine
50 how higher-order structure in brain data varies as a function of the cognitive richness of the stimulus.

51 Methods

52 There are two basic steps to our approach (Fig. 2). In the first step, we take a number-of-timepoints (T) by
53 number-of-features (F) *matrix of observations* (\mathbf{X}) and we return a T by $\frac{F^2-F}{2}$ *matrix of dynamic correlations* (\mathbf{Y}).
54 Here \mathbf{Y}_0 describes, at each moment, how all of the features (columns of \mathbf{X}) are inferred to be interacting.
55 (Since the interactions are assumed to be non-recurrent and symmetric, only the upper triangle of the full
56 correlation matrix is computed.) In the second step, we project \mathbf{Y}_0 onto an F -dimensional space, resulting in
57 a new T by F matrix \mathbf{Y}_1 . Note that \mathbf{Y}_1 contains information about the correlation dynamics present in \mathbf{X} , but
58 represented in a compressed number of dimensions. By repeatedly applying these two steps in sequence,
59 we can examine and explore higher order dynamic correlations in \mathbf{X} .

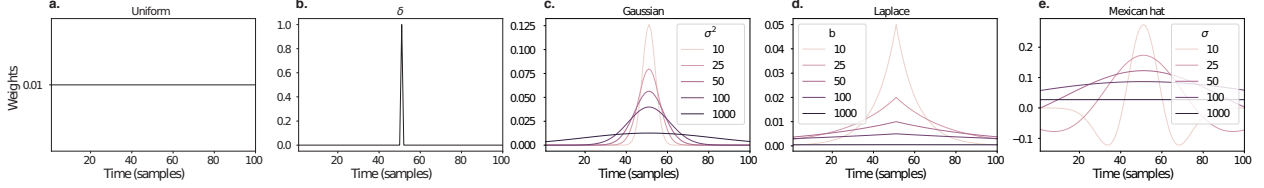


Figure 1: **Examples of time-varying weights.** Each panel displays per-timepoint weights at $t = 50$, evaluated for 100 timepoints (1, ..., 100). **a. Uniform weights.** The weights are timepoint-invariant; observations at all timepoints are weighted equally, and do not change as a function of t . This is a special case of weight function that reduces dynamic correlations to static correlations. **b. Dirac delta function.** Only the observation at timepoint t is given weight (of 1), and weights for observations at all other timepoints are set to 0. **c. Gaussian weights.** Each observation's weights fall off in time according to a Gaussian probability density function centered on $\mu = t$. Weights derived using several different example variance parameters (σ^2) are displayed. **d. Laplace weights.** Each observation's weights fall off in time according to a Laplace probability density function centered on $\mu = t$. Weights derived using several different example scale parameters (b) are displayed. **e. Mexican hat (Ricker wavelet) weights.** Each observation's weights fall off in time according to a Ricker wavelet centered on t . This function highlights the *contrasts* between local versus surrounding activity patterns in estimating dynamic correlations. Weights derived using several different example width parameters (σ) are displayed.

60 Dynamic correlations

Given a matrix of observations, we can compute the (static) correlations between any pair of observations, \mathbf{X}_i and \mathbf{X}_j using:

$$\text{corr}(\mathbf{X}_i, \mathbf{X}_j) = \frac{\sum_{t=1}^T (\mathbf{X}_i(t) - \bar{\mathbf{X}}_i)(\mathbf{X}_j(t) - \bar{\mathbf{X}}_j)}{\sqrt{\sum_{t=1}^T \sigma_{\mathbf{X}_i}^2 \sigma_{\mathbf{X}_j}^2}}, \text{ where} \quad (1)$$

$$\bar{\mathbf{X}}_k = \sum_{t=1}^T \mathbf{X}_k(t), \text{ and} \quad (2)$$

$$\sigma_{\mathbf{X}_k}^2 = \sum_{t=1}^T (\mathbf{X}_k(t) - \bar{\mathbf{X}}_k)^2 \quad (3)$$

61 We can generalize this formula to compute time-varying correlations by incorporating a *weight function*
62 that takes a time t as input, and returns how much the observed data every timepoint (including t) contribute
63 to the correlations at time t (Fig. 1).

Given a weight function $w(t)$ for timepoint t , evaluated at timepoints in the interval $[1, \dots, T]$, we can

extend the static correlation formula in Equation 2 to reflect an *instantaneous correlation* at timepoint t :

$$\text{timecorr}(\mathbf{X}_i, \mathbf{X}_j, t) = \frac{\sum_{t=1}^T (\mathbf{X}_i(t) - \tilde{\mathbf{X}}_i(t))(\mathbf{X}_j(t) - \tilde{\mathbf{X}}_j(t))}{\sqrt{\sum_{t=1}^T \tilde{\sigma}_{\mathbf{X}_i}^2(t) \tilde{\sigma}_{\mathbf{X}_j}^2(t)}}, \text{ where} \quad (4)$$

$$\tilde{\mathbf{X}}_k(t) = \sum_{i=1}^T w(t, i) \mathbf{X}_k(i), \quad (5)$$

$$\tilde{\sigma}_{\mathbf{X}_k}^2(t) = \sum_{i=1}^T (\mathbf{X}_k(i) - \tilde{\mathbf{X}}_k(t))^2, \quad (6)$$

and $w(t, i)$ is shorthand for $w(t)$ evaluated at timepoint i . Equation 5 may be used to estimate the instantaneous correlations between every pair of observations, at each timepoint (i.e., \mathbf{Y}).

66 Inter-subject dynamic correlations

Equation 5 provides a means of taking a single observation matrix, \mathbf{X} and estimating the dynamic correlations from moment to moment, \mathbf{Y} . Suppose that one has access to a set of multiple observation matrices that reflect the same phenomenon. For example, one might collect neuroimaging data from several experimental participants, as each participant performs the same task (or sequence of tasks). Let $\{\mathbf{X}_1, \mathbf{X}_2, \dots, \mathbf{X}_P\}$ reflect the T by F observation matrices for each of P participants in an experiment. We can use *inter-subject functional connectivity* (ISFC; Simony et al., 2016) to compute the degree of stimulus-driven correlations reflected in the multi-participant dataset at a given timepoint t using:

$$\bar{\mathbf{C}}(t) = M \left(R \left(\frac{1}{2P} \sum_{i=1}^P Z(Y_i(t))^T + Z(Y_i(t)) \right) \right), \quad (7)$$

where M extracts and vectorizes the diagonal and upper triangle of a symmetric matrix, Z is the Fisher z -transformation (Zar, 2010):

$$Z(r) = \frac{\log(1+r) - \log(1-r)}{2} \quad (8)$$

R is the inverse of Z :

$$R(z) = \frac{\exp(2z-1)}{\exp(2z+1)}, \quad (9)$$

and $\mathbf{Y}_i(t)$ denotes the correlation matrix (Eqn. 2) between each column of \mathbf{X}_i and each column of the average observations from all *other* participants, $\bar{\mathbf{X}}_{\setminus i}$:

$$\bar{\mathbf{X}}_{\setminus i} = R \left(\frac{1}{P-1} \sum_{i \in \setminus i} Z(\mathbf{X}_i) \right), \quad (10)$$

where $\setminus i$ denotes the set of all participants other than participant i . In this way, the T by $\left(\frac{F^2-F}{2} + F\right)$ matrix $\bar{\mathbf{C}}$ is the time-varying extension of the ISFC approach developed by Simony et al. (2016).

69 Higher-order correlations

Given a timeseries of dynamic correlations (e.g., obtained using Eqn. 5), higher-order correlations reflect the dynamic correlations between columns of \mathbf{Y} . Given unlimited computing resources, one could use repeated applications of Equation 5 to estimate these higher-order correlations (i.e., substituting in the previous output, \mathbf{Y} , for the input, \mathbf{X} in the equation). However, because each output \mathbf{Y} has $O(F^2)$ columns relative to F columns in the input \mathbf{X} , the output of Equation 5 grows with the square of the number of repeated applications (total cost of computing n^{th} order correlations is $O(F^{2n})$ for $n \in \mathcal{J}, n > 0$). When F or n is large, this approach quickly becomes intractable.

To make progress in computing \mathbf{Y}_{n+1} , we can approximate \mathbf{Y}_n by computing an $O(F)$ -dimensional embedding of \mathbf{Y}_n , termed $\hat{\mathbf{Y}}_n$, and then we can apply Equation 5 to $\hat{\mathbf{Y}}_n$ rather than directly to \mathbf{Y}_n . This enables us to maintain $O(n)$ scaling with respect to n , rather than exponential scaling via the direct approach.

There are many possible methods for computing $\hat{\mathbf{Y}}_n$ from \mathbf{Y}_n , including traditional dimensionality reduction approaches and graph theory based approaches as described next. In the *Discussion* section we elaborate on other potential approaches.

83 Dimensionality reduction-based approaches to computing $\hat{\mathbf{Y}}_n$

Commonly used dimensionality reduction algorithms include Principal Components Analysis (PCA; Pearson, 1901), Probabilistic PCA (PPCA; Tipping & Bishop, 1999), Exploratory Factor Analysis (EFA; Spearman, 1904), Independent Components Analysis (ICA; Jutten & Herault, 1991; Comon et al., 1991), t -Stochastic Neighbor Embedding (t -SNE; van der Maaten & Hinton, 2008), Uniform Manifold Approximation and Projection (UMAP; McInnes & Healy, 2018), non-negative matrix factorization (NMF; Lee & Seung, 1999), Topographic Factor Analysis (TFA) Manning et al. (2014), Hierarchical Topographic Factor analysis (HTFA) Manning et al. (2018), Topographic Latent Source Analysis (TLSA) Gershman et al. (2011), Dictionary learning (J. B. Mairal et al., 2009; J. Mairal et al., 2009), deep autoencoders (Hinton & Salakhutdinov,

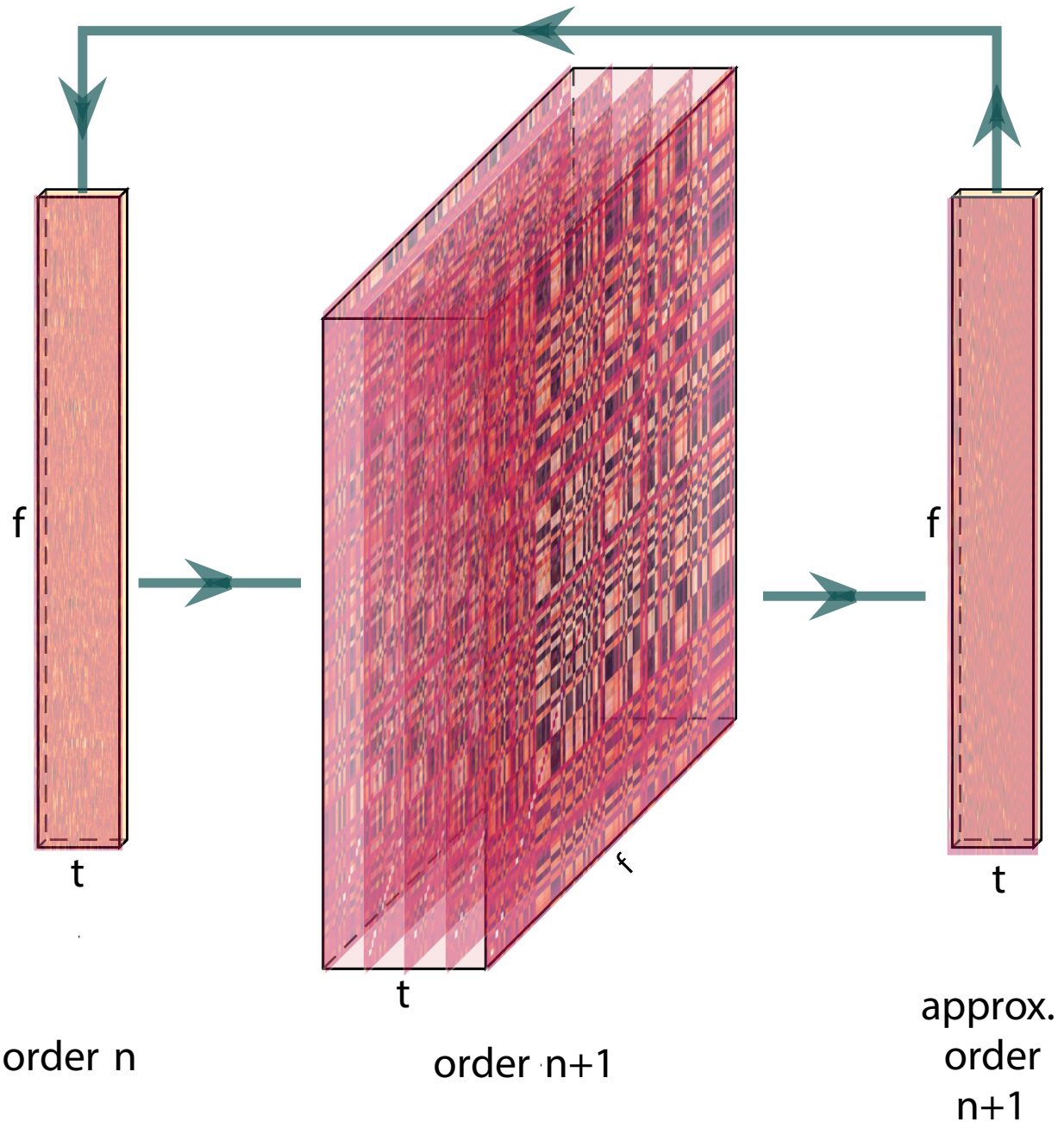


Figure 2: **Computing higher order correlations.** Correlations are computed then approximated to the same size as original data. This process is repeated to computer

92 among others. While complete characterizations of each of these algorithms is beyond the scope of
93 the present manuscript, the general intuition driving these approaches is to compute the $\hat{\mathbf{Y}}$ with i columns
94 that is closest to the original \mathbf{Y} with j columns, and where (typically) $i \ll j$. The different approaches place
95 different constraints on what properties $\hat{\mathbf{Y}}$ must satisfy and which aspects of the data are compared (and
96 how) to characterize the match between $\hat{\mathbf{Y}}$ and \mathbf{Y} .

97 Applying dimensionality reduction algorithms to \mathbf{Y} yields a $\hat{\mathbf{Y}}$ whose columns reflect weighted combi-
98 nations (or nonlinear transformations) of the original columns of \mathbf{Y} . This has two main consequences. First,
99 with each repeated dimensionality reduction, the resulting $\hat{\mathbf{Y}}_n$ has lower and lower fidelity (with respect to
100 what the “true” \mathbf{Y}_n might have looked like without using dimensionality reduction to maintain scalability).
101 In other words, computing $\hat{\mathbf{Y}}_n$ is a lossy operation. Second, whereas the columns of \mathbf{Y}_n may be mapped
102 directly onto pairs of columns of \mathbf{Y}_{n-1} , that mapping either becomes less cleanly defined in $\hat{\mathbf{Y}}_n$ due to the
103 reweightings and/or nonlinear transformations.

104 **Graph theory-based approaches to computing $\hat{\mathbf{Y}}_n$**

105 Graph theoretic measures take as input a matrix of interactions (e.g., using the above notation, an $F \times F$
106 correlation matrix or binarized correlation matrix reconstituted from a single timepoint’s row of \mathbf{Y}) and
107 return as output a set of F measures describing how each node (feature) sits within that interactions matrix
108 with respect to the rest of the population. Common measures include betweenness centrality (the proportion
109 of shortest paths between each pair of nodes in the population that involves the given node in question; e.g.,
110 Newman, 2005; Opsahl et al., 2010; Barthélemy, 2004; Geisberger et al., 2008; Freeman, 1977); diversity and
111 dissimilarity (characterizations of how differently connected a given node is from others in the population;
112 e.g., Rao, 1982; Lin, 2009; Ricotta & Szeidl, 2006); Eigenvector centrality and pagerank centrality (measures of
113 how influential a given node is within the broader network; e.g., Newman, 2008; Bonacich, 2007; Lohmann
114 et al., 2010; Halu et al., 2013); transfer entropy and flow coefficients (a measure of how much information is
115 flowing from a given node to other nodes in the network; e.g., Honey et al., 2007; Schreiber, 2000); k -coreness
116 centrality (a measure of the connectivity of a node within its local sub-graph; e.g., Alvarez-Hamelin et al.,
117 2005; Christakis & Fowler, 2010); within-module degree (a measure of how many connections a node has to
118 its close neighbors in the network; e.g., Rubinov & Sporns, 2010); participation coefficient (a measure of the
119 diversity of a node’s connections to different sub-graphs in the network; e.g., Rubinov & Sporns, 2010); and
120 sub-graph centrality (a measure of a node’s participation in all of the network’s sub-graphs; e.g., Estrada &
121 Rodríguez-Velázquez, 2005).

122 As an alternative to the above dimensionality reduction approach to embedding \mathbf{Y}_n in a lower-dimensional

space, but still allowing for scalable explorations of higher-order structure in the data, we also explore using the above graph theoretic measures as a means of obtaining $\hat{\mathbf{Y}}_n$. In particular: for a given graph theoretic measure, $\eta : \mathcal{R}^{F \times F} \rightarrow \mathcal{R}^F$, we can use η to transform each row of \mathbf{Y}_n in a way that characterizes the corresponding graph-theoretic properties of each column. Whereas the dimensionality reduction approach to computing $\hat{\mathbf{Y}}_n$ is lossy, the graph-theory approach is lossless. However, whereas the dimensionality reduction approach maintains ties (direct or indirect) to the original activity patterns reflected in \mathbf{Y}_{n-1} , the graph-theory approach does not. Instead, the graph-theory characterizes the nature and timecourse of each feature's *participation* in the network.

131 Evaluation metrics

132 We evaluate our approach to extracting dynamic correlations and higher-order correlations using several
133 metrics detailed next. First, we generated synthetic data using known time-varying correlations, and then
134 we evaluated the fidelity with which Equation 5 could recover those correlations (for synthetic datasets
135 with different properties, and using different kernels to define the weights; Fig. 1). We then turned to a
136 series of analyses on a (real) neuroimaging dataset where the ground truth correlations were *not* known.
137 We evaluated whether the recovered correlations could be used to accurately label held-out neuroimaging
138 data with the time at which it was collected. We used this latter evaluations (using timepoint decoding)
139 as a proxy for gauging how much explanatory power the recovered correlations held with respect to the
140 observed data.

141 Generating synthetic data

142 Ramping dataset and block dataset. Add details (Fig. 3)

143 Recovery of ground truth parameters from synthetic data

144 To explore recovery of a constant correlation, we created a random correlation matrix and added a
145 small amount of Gaussian noise to

146 We applied timecorr with a given kernel (Fig. 1) to synthetic data, then correlate each recovered correlation
147 matrix with the ground truth. Explore how recovery varies with the kernel, kernel parameters, and specific
148 structure of the data (e.g. slow changes as in the ramping dataset, versus rapid changes as in the block
149 dataset).

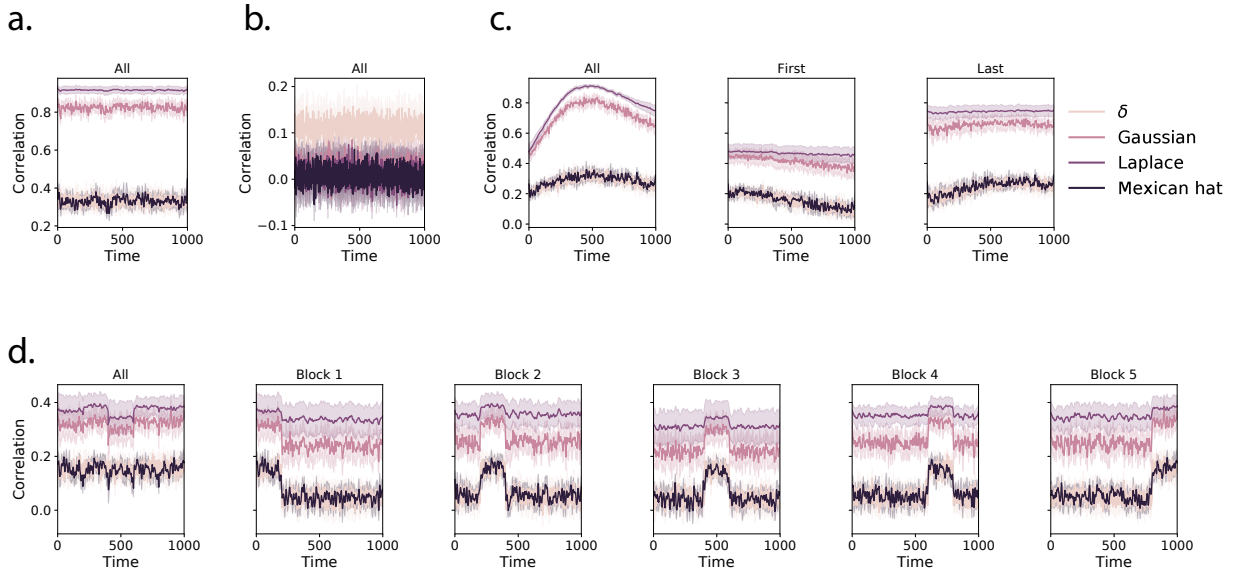


Figure 3: Dynamic correlation recovery with synthetic data. **a.** Recovery using a constant dataset. Using constant dataset, how well can we recover using different kernels. **b.** Recovery using random dataset. **c.** Ramping recovery. **d.** Block recovery

150 Timepoint decoding

151 To explore how higher-order structure varies with stimulus structure and complexity, we used a previous
 152 neuroimaging dataset Simony et al. (2016) in which participants listened to an audio recording of a story;
 153 36 participants listen to an intact version of the story, 17 participants listen to time-scrambled recordings of
 154 the same story where paragraphs were scrambled, 36 participants listen to word-scrambled version and 36
 155 participants lay in rest condition.

156 Prior work has shown participants share similar neural responses to richly structured stimuli when
 157 compared to stimuli with less structure. To assess whether the moment-by-moment higher order correlations
 158 were reliably preserved across participants, we used inter-subject functional connectivity (ISFC) to isolate
 159 the time-varying correlational structure (functional connectivity patterns that were specifically driven by
 160 the story participants listened to. Following the analyses conducted by (HTFA) Manning et al. (2018), we
 161 first applied *hierarchical topographic factor analysis* (HTFA) to the fMRI datasets to obtain a time series of
 162 700 node activities for every participant. We then computed the dynamic weighted ISFC using a gaussian
 163 kernel with a width of 5. We then approximated these dynamic correlation using PCA and computed the
 164 dynamic weighted ISFC on the approximations. We repeated this process up to 10th order approximated
 165 correlations.

166 To assess decoding accuracy, we randomly divided participants for each stimulus into training and

167 testing groups. For the zeroth order, we computed the mean factor activity for each group. For all subsequent
168 orders up to the tenth order, we computed the mean approximated dynamic ISFC of factor activity for each
169 group. To assess how additional higher-order correlations contribute to decoding accuracy, for each order
170 we included a weighted-mixture (described below) of the activity patterns of all previous orders. For each
171 group of participants in turn, we compared these activity patterns (using Pearson correlations) to estimate
172 the story times each pattern corresponded to. Specifically, we asked, for each timepoint: what are the
173 correlations between the first group's and second group's activity patterns at each order. We note that the
174 decoding test we used is a conservative in which we count a timepoint label as incorrect if it is not an exact
175 match.

176 For each order we obtained the weighted-mixture of the correlation matrices for the current order and
177 all previous orders using mixing parameter ϕ , where $0 < \phi < 1$ reflects a weighted mixture of order
178 based decoding Fig. ?? Panel C.). We calculated ϕ , by subdividing the training group and using the quasi-
179 Newton method of Broyden, Fletcher, Goldfarb, and Shanno (BFGS) for optimization. We repeated this
180 cross-validation process 100 times.

181 Results

182 Synthetic data

183 Figure: overall timecourse of recovery, also recovery near event boundaries.

184 Neuroimaging dataset (Simony et al., 2016)

185 For our decoding analysis, we used HTFA-derived node activities Manning et al. (2018) from fMRI data
186 collected as participants listened to an audio recording of a story (intact condition; 36 participants), lis-
187 tened to time scrambled recordings of the same story (17 participants in the paragraph-scrambled condition
188 listened to the paragraphs in a randomized order and 36 in the word-scrambled condition listened to
189 the words in a randomized order), or lay resting with their eyes open in the scanner (rest condition; 36
190 participants). We sought to demonstrate how higher-order correlations may be used to examine dynamic
191 interactions of brain patterns in (real) multi-subject fMRI datasets. This story listening dataset was col-
192 lected as part of a separate study, where the full imaging parameters, image preprocessing methods, and
193 experimental details may be found (Simony et al., 2016). The dataset is available at <http://arks.princeton.edu/ark:/88435/dsp015d86p269k>. Bars of each color display cross-validated decoding performance for
194 decoders trained using different sets of neural features: whole-brain patterns of voxel activities
195

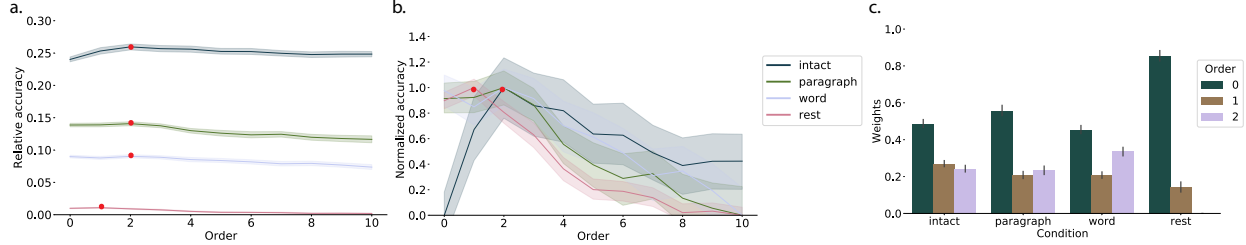


Figure 4: Decoding by order. **a. Relative decoding accuracy by order.** Ribbons of each color display cross-validated decoding performance for each condition (intact, paragraph, word, and rest). Decoders were trained using increasingly more higher-order information and this ribbons are displayed relative to chance at 0. The red dots indicates maximum decoding accuracy for each condition. **b. Normalized decoding accuracy by order.** We normalized the decoding accuracy by order to better visualize the order with the maximum decoding accuracy for each condition. **c. Optimized weights.** Bar heights indicate the optimized mixing parameter ϕ of each contributing order up to and including the order with the maximum decoding accuracy for each contributing order. For the order with maximum decoding accuracy by condition, we show barplots of the optimized weights ϕ for each contributing order.

196 We next evaluated if our model of high-order correlations in brain activity can capture cognitively
 197 relevant brain patterns. We performed a decoding analysis, using cross validation to estimate (using other
 198 participants' data) which parts of the story each weighted-mixture of higher-order brain activity pattern
 199 corresponded to (see *Materials and methods*). We note that our primary goal was not to achieve perfect
 200 decoding accuracy, but rather to use decoding accuracy as a benchmark for assessing whether different
 201 neural features specifically capture cognitively relevant brain patterns.

202 Separately for each experimental condition, we divided participants into two groups. For the zeroth
 203 order, we computed the mean factor activity for each group. For all subsequent orders up to the tenth
 204 order, we computed the mean approximated dynamic ISFC of factor activity for each group (see *Materials*
 205 and *methods*), and combined in a weighted mixutre with all previous orders (i.e. cross-validation for the
 206 second order contained a weighted-mixture of zeroth, first, and second order c. **Optimized weights.**) For
 207 each order, we correlated the group 1 activity patterns with group 2 activity patterns. We then subdivided
 208 the group 1 to obtain an optimal weighting parameter for each order's correlation matrix using the same
 209 cross validation method. We used the optimal weighting parameters to obtain a weighted-mixture (see
 210 *Materials and methods*) of each order's correlation matrix. Using these correlations, we labeled the group 1
 211 timepoints using the group 2 timepoints with which they were most highly correlated; we then computed
 212 the proportion of correctly labeled group 1 timepoints. (We also performed the symmetric analysis whereby
 213 we labeled the group 2 timepoints using the group 1 timepoints as a template.) We repeated this procedure
 214 100 times (randomly re-assigning participants to the two groups each time) to obtain a distribution of
 215 decoding accuracies for each experimental condition. (There were 272 timepoints for paragraph condition,
 216 300 timepoints for intact and word conditions, and 400 timepoints for rest condition, so chance performance

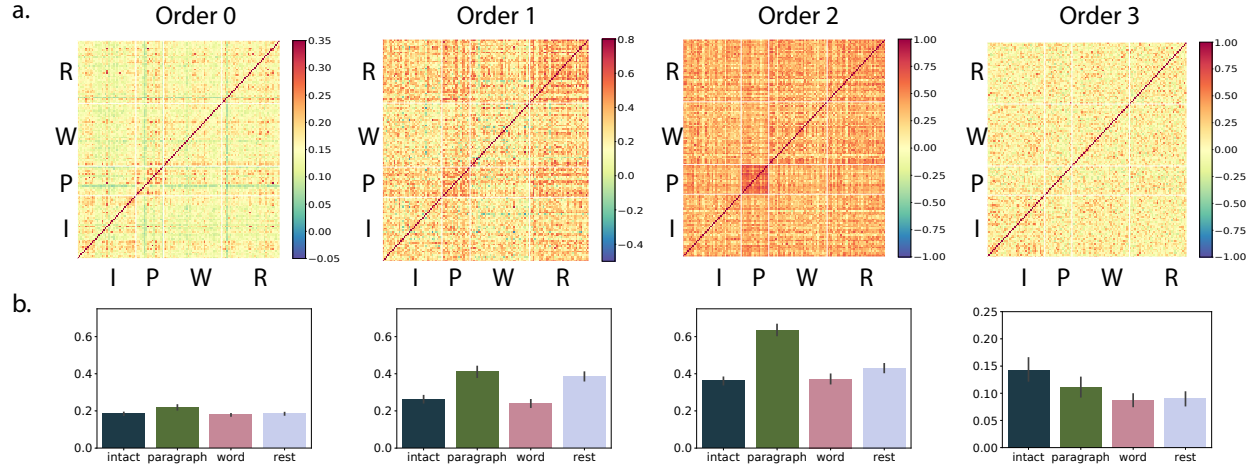


Figure 5: Inter-subject correlations by order. **a. Inter-subject correlation heatmaps by order.** Heatmaps for each order of how correlated each subject is with every other subject grouped by condition (intact (I), paragraph (P), word (W), and rest (R)). **b. Mean correlation for each condition by order.** Bar heights indicate inter-subject correlations by condition for each order.

217 on this decoding test is was $\frac{1}{272}$, $\frac{1}{300}$, and $\frac{1}{400}$ respectively.

218 Discussion

- 219 • Decoding accuracy best for level 2 data for all but rest condition. Could be that the brain is 2nd order
220 or that fMRI can only reliable give 2nd order.
- 221 • multiple timescale representations (a la Hasson group) implies first-order network interactions.
222 higher-order interactions imply generalizations between interacting representations (e.g. mirrored
223 schema, a la Norman/Baldassano/Hasson). possibly cite NTB 2013 science review, using as evidence
224 that this is where the field is going (voxels → patterns (L0) → interactions (L1) → higher order patterns
225 (L2+)).
- 226 • related approaches: sliding window, phase-based correlations, within-ROI spatial correlations at each
227 timepoint, granger causality, other explit models (e.g. virtual brain).
- 228 • other applications: molecular interactions (protein folding?), diagnosis (e.g. psychiatric disorders
229 as network flow problems- grattan work?), social network dynamics (e.g. financial markets, social
230 media interactions)

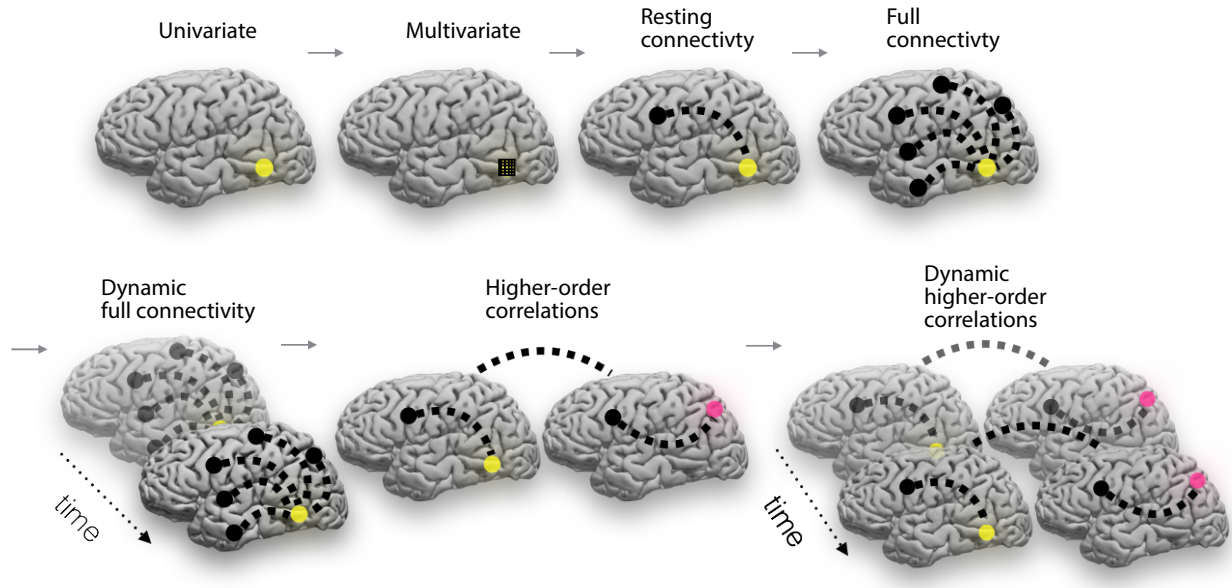


Figure 6: **Direction of the field.**

²³¹ **Concluding remarks**

²³² the universe is complicated and we need scalable approaches to studying how the pieces are interacting to
²³³ make sense of it. one small step for mankind, and so on.

²³⁴ **Acknowledgements**

²³⁵ We acknowledge discussions with Luke Chang, Hany Farid, Paxton Fitzpatrick, Andrew Heusser, Eshin
²³⁶ Jolly, Qiang Liu, Matthijs van der Meer, Judith Mildner, Gina Notaro, Stephen Satterthwaite, Emily Whitaker,
²³⁷ Weizhen Xie, and Kirsten Ziman. Our work was supported in part by NSF EPSCoR Award Number 1632738
²³⁸ to J.R.M. and by a sub-award of DARPA RAM Cooperative Agreement N66001-14-2-4-032 to J.R.M. The
²³⁹ content is solely the responsibility of the authors and does not necessarily represent the official views of our
²⁴⁰ supporting organizations.

²⁴¹ **Author contributions**

²⁴² Concept: J.R.M. Implementation: T.H.C., L.L.W.O., and J.R.M. Analyses: L.L.W.O and J.R.M.

243 References

- 244 Alvarez-Hamelin, I., Dall'Asta, L., Barrat, A., & Vespignani, A. (2005). *k*-corr decomposition: a tool for the
245 visualization of large scale networks. *arXiv*, cs/0504107v2.
- 246 Barthélemy, M. (2004). Betweenness centrality in large complex networks. *European Physical Journal B*, 38,
247 163–168.
- 248 Bonacich, P. (2007). Some unique properties of eigenvector centrality. *Social Networks*, 29(4), 555–564.
- 249 Christakis, N. A., & Fowler, J. H. (2010). Social network sensors for early detection of contagious outbreaks.
250 *PLoS One*, 5(9), e12948.
- 251 Comon, P., Jutten, C., & Herault, J. (1991). Blind separation of sources, part II: Problems statement. *Signal
252 Processing*, 24(1), 11 - 20.
- 253 Estrada, E., & Rodríguez-Velázquez, J. A. (2005). Subgraph centrality in complex networks. *Physical Review
254 E*, 71(5), 056103.
- 255 Freeman, L. C. (1977). A set of measures of centrality based on betweenness. *Sociometry*, 40(1), 35–41.
- 256 Geisberger, R., Sanders, P., & Schultes, D. (2008). Better approximation of betweenness centrality. *Proceedings
257 of the meeting on Algorithm Engineering and Experiments*, 90–100.
- 258 Gershman, S., Blei, D., Pereira, F., & Norman, K. (2011). A topographic latent source model for fMRI data.
259 *NeuroImage*, 57, 89–100.
- 260 Halu, A., Mondragón, R. J., Panzarasa, P., & Bianconi, G. (2013). Multiplex PageRank. *PLoS One*, 8(10),
261 e78293.
- 262 Hinton, G. E., & Salakhutdinov, R. R. (2006). Reducing the dimensionality of data with neural networks.
263 *Science*, 313(5786), 504–507.
- 264 Honey, C. J., Kötter, R., Breakspear, M., & Sporns, O. (2007). Network structure of cerebral cortex shapes
265 functional connectivity on multiple time scales. *Proceedings of the National Academy of Science USA*, 104(24),
266 10240–10245.
- 267 Jutten, C., & Herault, J. (1991). Blind separation of sources, part I: An adaptive algorithm based on
268 neuromimetic architecture. *Signal Processing*, 24(1), 1–10.
- 269 Lee, D. D., & Seung, H. S. (1999). Learning the parts of objects by non-negative matrix factorization. *Nature*,
270 401, 788–791.

- 271 Lin, J. (2009). Divergence measures based on the Shannon entropy. *IEEE Transactions on Information Theory*,
272 37(1), 145–151.
- 273 Lohmann, G., Margulies, D. S., Horstmann, A., Pleger, B., Lepsien, J., Goldhahn, D., ... Turner, R. (2010).
274 Eigenvector centrality mapping for analyzing connectivity patterns in fMRI data of the human brain.
275 *PLoS One*, 5(4), e10232.
- 276 Mairal, J., Ponce, J., Sapiro, G., Zisserman, A., & Bach, F. R. (2009). Supervised dictionary learning. *Advances
277 in Neural Information Processing Systems*, 1033–1040.
- 278 Mairal, J. B., Bach, F., Ponce, J., & Sapiro, G. (2009). Online dictionary learning for sparse coding. *Proceedings
279 of the 26th annual international conference on machine learning*, 689–696.
- 280 Manning, J. R., Ranganath, R., Norman, K. A., & Blei, D. M. (2014). Topographic factor analysis: a Bayesian
281 model for inferring brain networks from neural data. *PLoS One*, 9(5), e94914.
- 282 Manning, J. R., Zhu, X., Willke, T. L., Ranganath, R., Stachenfeld, K., Hasson, U., ... Norman, K. A. (2018).
283 A probabilistic approach to discovering dynamic full-brain functional connectivity patterns. *NeuroImage*,
284 180, 243–252.
- 285 McInnes, L., & Healy, J. (2018). UMAP: Uniform manifold approximation and projection for dimension
286 reduction. *arXiv*, 1802(03426).
- 287 Newman, M. E. J. (2005). A measure of betweenness centrality based on random walks. *Social Networks*, 27,
288 39–54.
- 289 Newman, M. E. J. (2008). The mathematics of networks. *The New Palgrave Encyclopedia of Economics*, 2, 1–12.
- 290 Opsahl, T., Agneessens, F., & Skvoretz, J. (2010). Node centrality in weighted networks: generalizing degree
291 and shortest paths. *Social Networks*, 32, 245–251.
- 292 Pearson, K. (1901). On lines and planes of closest fit to systems of points in space. *The London, Edinburgh,
293 and Dublin Philosophical Magazine and Journal of Science*, 2, 559–572.
- 294 Rao, C. R. (1982). Diversity and dissimilarity coefficients: a unified approach. *Theoretical Population Biology*,
295 21(1), 24–43.
- 296 Ricotta, C., & Szeidl, L. (2006). Towards a unifying approach to diversity measures: Bridging the gap
297 between the Shannon entropy and Rao's quadratic index. *Theoretical Population Biology*, 70(3), 237–243.

- 298 Rubinov, M., & Sporns, O. (2010). Complex network measures of brain connectivity: uses and interpreta-
299 tions. *NeuroImage*, 52, 1059–1069.
- 300 Schreiber, T. (2000). Measuring information transfer. *Physical Review Letters*, 85(2), 461–464.
- 301 Simony, E., Honey, C. J., Chen, J., & Hasson, U. (2016). Uncovering stimulus-locked network dynamics
302 during narrative comprehension. *Nature Communications*, 7(12141), 1–13.
- 303 Spearman, C. (1904). General intelligence, objectively determined and measured. *American Journal of
304 Psychology*, 15, 201–292.
- 305 Tipping, M. E., & Bishop, C. M. (1999). Probabilistic principal component analysis. *Journal of Royal Statistical
306 Society, Series B*, 61(3), 611–622.
- 307 van der Maaten, L. J. P., & Hinton, G. E. (2008). Visualizing high-dimensional data using t-SNE. *Journal of
308 Machine Learning Research*, 9, 2579–2605.
- 309 Zar, J. H. (2010). *Biostatistical analysis*. Prentice-Hall/Pearson.